

Systematic estimation of theoretical uncertainties in the calculation of the pion-photon transition form factor using light-cone sum rules

S. V. Mikhailov,^{1,*} A. V. Pimikov,^{1,2,†} and N. G. Stefanis^{3,‡}

¹*Bogoliubov Laboratory of Theoretical Physics, JINR, 141980 Dubna, Russia*

²*Institute of Modern Physics, Chinese Academy of Sciences, Lanzhou, 730000, P. R. China*

³*Institut für Theoretische Physik II, Ruhr-Universität Bochum, D-44780 Bochum, Germany*

(Dated: October 8, 2018)

We consider the calculation of the pion-photon transition form factor $F^{\gamma^*\gamma\pi^0}(Q^2)$ within light-cone sum rules focusing attention to the low-mid region of momenta. The central aim is to estimate the theoretical uncertainties which originate from a wide variety of sources related to (i) the relevance of next-to-next-to-leading order radiative corrections (ii) the influence of the twist-four and the twist-six term (iii) the sensitivity of the results on auxiliary parameters, like the Borel scale M^2 , (iv) the role of the phenomenological description of resonances, and (v) the significance of a small but finite virtuality of the quasireal photon. Predictions for $F^{\gamma^*\gamma\pi^0}(Q^2)$ are presented which include all these uncertainties and found to comply within the margin of experimental error with the existing data in the Q^2 range between 1 and 5 GeV², thus justifying the reliability of the applied calculational scheme. This provides a solid basis for confronting theoretical predictions with forthcoming data bearing small statistical errors.

PACS numbers: 12.38.Lg, 12.38.Bx, 13.40.Gp

I. INTRODUCTION

During the last years, several experimental groups have reported data on the pion-photon transition form factor (TFF). Typically, these B factory experiments are single-tag $\gamma^*(q_1)\gamma(q_2) \rightarrow \pi^0(P)$ measurements in which one of the two photons has a very small virtuality $q_2^2 \rightarrow 0$, inherited by the untagged electron, while the other photon is highly off shell. Therefore, the TFF measured in such an experimental setup is a function of one — the large $q_1^2 = -Q^2$ — photon virtuality, $F_{\gamma\pi}(Q^2)$. The recent theoretical interest focused primarily on the BABAR experiment (2009) [1] because of two reasons. First, because it extended the range of data to quite high Q^2 values of the order of 40 GeV² and, second, because just these high- Q^2 data were found to increase with the momentum Q^2 — an unexpected result within the collinear factorization scheme of quantum chromodynamics (QCD) [2, 3]. The subsequent Belle experiment (2012) [4] covered the same domain of momenta with similar precision, but did not confirm the rising trend of the scaled $\pi\gamma$ TFF at high Q^2 , with most data points being in agreement with the hard-scattering limit of QCD.

Several theoretical groups have attempted to provide explanations for the auxetic¹ behavior of the high-precision BABAR data presuming that these are also accurate, i.e., true values and not the result of a false mea-

surement. These efforts range from approaches with the sole aim to provide after-the-fact rationalizations of such an anomalous increase of the scaled form factor [6–9] — to name just a few — to analyses arguing that the auxetic behavior of the BABAR data above ~ 10 GeV² is incompatible with QCD and cannot be reproduced by predictions obtained herewith see, for example, [5, 10–15]. Under this particular perspective, the high- Q^2 BABAR data are — in the statistical sense — precise but not accurate because they fail to cluster around the ultraviolet (UV) limit, $Q^2 F^{\gamma^*\gamma\pi^0}(Q^2 \rightarrow \infty, 0) = \sqrt{2}f_\pi$ GeV, which is an exact result of QCD [3, 16]. Still other theorists [17, 18] argue that a best-fit to *all* high- Q^2 data (Belle and BABAR), being somewhere in between (see [12] for a classification scheme of theoretical predictions), would only show a moderate increase of the scaled TFF at currently accessible momenta so that this enhancement could still be accommodated within the standard framework of QCD based on collinear factorization without the need to invoke unconventional nonperturbative mechanisms. This treatment, they say, is justifiable, given that the relative deviation between the Belle and the BABAR data fits does not exceed $1.5\sigma - 2\sigma$ [4]. Moreover, it is not a priori known at which Q^2 values the TFF should reach the asymptotic limit either from below or from above. The issue around the incongruent trends of the high- Q^2 measurements may be resolved after 2018 when the BelleII experiment at the SuperKEKB collider in Japan will start collecting high-precision data on two-photon physics, see, e.g., [19], so that the correct behavior of the TFF at large momenta $Q^2 F^{\gamma^*\gamma\pi^0}(Q^2 \gg 1\text{GeV}^2, 0)$ can be estimated more rigorously, eventually reducing the range of multi-layered theoretical predictions to a single reliable curve within a comparably small margin of systematic theoretical error [12].

*Electronic address: mikhs@theor.jinr.ru

†Electronic address: pimikov@theor.jinr.ru

‡Electronic address: stefanis@tp2.ruhr-uni-bochum.de

¹ The term auxetic was introduced and explained in [5]. In the following it is used to describe the deviation from the hard-scattering limit of QCD following from collinear factorization.

Despite this debate at the high-end of the probed momentum values in the measurement of the pion-photon TFF also the mid-low- Q^2 region is of particular importance. The reason is that the available data sets obtained in the range $[1 - 5] \text{ GeV}^2$ nearby the modern normalization scale $\mu_0 = 2 \text{ GeV}$, used in lattice simulations and other calculations [20–22], have rather large errors so that they cannot be used to fine-tune theoretical predictions in this domain. This applies to the CELLO [23] data and partially also to the CLEO [24] data. The situation is expected to improve significantly when the data of the BESIII Collaboration, taken with the single-tag technique at $\sqrt{s} = 3.770 \text{ GeV}$ with the BESIII detector at the BEPCII collider, will become available. The process under study is $e^+e^- \rightarrow e^+e^- \text{hadron(s)}$, where either the electron or positron in the final state is detected. However, for the time being, only simulated data in the range $Q^2 \in [0.5 - 3] \text{ GeV}^2$ have been publicized which mainly serve to demonstrate the small size of the experimental errors in the event analysis [25]. Assuming as a pretext that the BESIII Collaboration will indeed provide real data with very small statistical errors in the spacelike region $Q^2 \lesssim 4 \text{ GeV}^2$, we may attempt to quantify how the existence of such data might be used to confront in more detail the theoretical systematic uncertainties, pertinent to the employed calculational method in this momentum regime. Such dedicated theoretical investigations have been carried out before within particular approaches. These include soft QCD modeling based on a set of Dyson-Schwinger equations (DSE) truncated to the ladder-rainbow level [26], or employ ideas related to the vector-meson dominance and the Padé approximation [27]. In a more recent work, the pion TFF was calculated by means of a dispersive approach in terms of the most important intermediate states [28]. The small to medium Q^2 region was also addressed within AdS/QCD using a holographic confining model in terms of an effective interaction in light-front time [14]. In the context of the light-cone sum-rule (LCSR) method such analysis has not yet been carried out and is part of the present investigation.

Several challenging questions arise: (i) How significant is the inclusion of higher twists, e.g., twist-four and twist six, at scales around $1\text{--}2 \text{ GeV}^2$ relative to the leading twist-two term? (ii) Are radiative corrections at the next-to-next-to-leading order (NNLO) level relevant at such low momentum scales? (iii) How reliable are light-cone sum rules for the calculation of $F_{\gamma\pi}(Q^2)$ in the $Q^2 \sim 1 \text{ GeV}^2$ region? (iv) How strong is the influence of the finite virtuality of the quasisreal photon at such scales? This work seeks quantitative answers to these questions.

The plan of the paper is the following. In the next section, we will examine the pion-photon TFF making use of QCD factorization to be followed in Sec. III by its formulation in the framework of LCSRs. To incorporate the nonperturbative input of the pion bound state of twist

two, the BMS² distribution amplitudes (DA)s and the platykurtic DA [21, 22] will be used. The main radiative corrections (up to the NNLO level) and the key higher-twist contributions (twist-four and twist six) to the TFF will be considered in Sec. IV. Section V is devoted to the comparison of the obtained predictions with the low- Q^2 data, the particular emphasis being placed on the new elements of our upgraded theoretical framework and the estimation of the most crucial systematic uncertainties. A summary of our findings and our conclusions will be given in Sec. VI. Some important technical ingredients of the approach are provided in two appendices.

II. PION-PHOTON TRANSITION FORM FACTOR USING QCD FACTORIZATION

Let us begin our analysis by considering the process $\gamma^*(q_1^2)\gamma(q_2^2) \rightarrow \pi^0$, with $q_1^2 = -Q^2$ for the far-off shell photon and $q_2^2 = -q^2 \gtrsim 0$ for the quasisreal photon, described by the pion-photon transition form factor

$$\int d^4z e^{-iq_1 \cdot z} \langle \pi^0(P) | T \{ j_\mu(z) j_\nu(0) \} | 0 \rangle = i \epsilon_{\mu\nu\alpha\beta} q_1^\alpha q_2^\beta \times F^{\gamma^* \gamma^* \pi^0}(Q^2, q^2), \quad (1)$$

where j_μ is the quark electromagnetic current. Employing perturbative QCD (pQCD) in connection with collinear factorization, the leading-twist two TFF for two highly off-shell photons, $F^{\gamma^* \gamma^* \pi^0}(Q^2, q^2; \mu_F^2)$, can be cast in convolution form at the factorization scale μ_F^2 to read

$$F^{\gamma^* \gamma^* \pi^0}(Q^2, q^2; \mu_F^2) = T(Q^2, q^2; \mu_F^2; x) \otimes \varphi_\pi^{(2)}(x, \mu_F^2). \quad (2)$$

Here, $\otimes \equiv \int_0^1 dx$ and $\varphi_\pi^{(2)}(x, \mu_F^2)$ denotes the pion distribution amplitude of leading twist two. It describes the partition of longitudinal-momentum fractions between the valence quark ($x_q = x = (k^0 + k^3)/(P^0 + P^3) = k^+/P^+$) and antiquark ($x_{\bar{q}} = 1 - x \equiv \bar{x}$) at the scale μ_F . The hard-scattering amplitude T can be expressed as a power-series expansion in the running strong coupling $a_s \equiv \alpha_s(\mu_R^2)/4\pi$ to obtain

$$T(Q^2, q^2; \mu_F^2; x) = T_{\text{LO}} + a_s T_{\text{NLO}} + a_s^2 T_{\text{NNLO}} + \dots, \quad (3)$$

where we have adopted the so-called default scale setting in which the renormalization scale μ_R is set equal to the factorization scale μ_F , i.e., $a_s(\mu_R^2) = a_s(\mu_F^2)$. We have also used for convenience the following abbreviations: LO — leading order, NLO — next-to-leading order, and NNLO — next-to-next-to-leading order. The corresponding contributions will be labeled by the superscripts (0), (1), and (2), respectively; they indicate the power of the strong coupling a_s .

² The acronym BMS is a reference to the authors of Ref. [29].

The various terms in (3) are given by the following expressions

$$T_{\text{LO}} = T_0, \quad (4a)$$

$$T_{\text{NLO}} = C_F T_0 \otimes [\mathcal{T}^{(1)} + L V_+^{(0)}], \quad (4b)$$

$$T_{\text{NNLO}} = C_F T_0 \otimes \left[\mathcal{T}^{(2)} + L V_+^{(1)}/C_F - L \beta_0 \mathcal{T}^{(1)} - \frac{L^2}{2} \beta_0 V_+^{(0)} + \frac{L^2}{2} C_F V_+^{(0)} \otimes V_+^{(0)} + L C_F \mathcal{T}^{(1)} \otimes V_+^{(0)} \right], \quad (4c)$$

in which we have introduced the convenient abbreviation $L \equiv \ln[(Q^2 y + q^2 \bar{y})/\mu_F^2]$, see [30]. Each term of the hard-scattering amplitude comprises several contributions originating from different sources. A common factor is the lowest-order (Born) term, viz., $T_0(Q^2, q^2; y)$, while $\mathcal{T}^{(1)}(y, x)$ and $\mathcal{T}^{(2)}(y, x)$ represent the coefficient functions of the considered partonic subprocess. The NLO contribution T_{NLO} in Eq. (4b) is completely known [30, 31]. On the other hand, the NNLO correction T_{NNLO} (see Eq. (4c)) contains the quantities $V^{(0)}(y, x)$ and $V^{(1)}(y, x)$, which denote, respectively, the one- and two-loop kernels of the Efremov-Radyushkin-Brodsky-Lepage (ERBL) [2, 3] evolution equation. Their structures are displayed explicitly in Appendix A, using for $V_+^{(1)}$ a new more compact representation, derived in this work, which is given by Eq. (A1). Note that β_0 is the first coefficient of the QCD β -function displayed in Eq. (A8). Furthermore, we isolate the important term T_β [10], which accumulates all terms proportional to β_0 on the RHS of Eq. (4c), to obtain

$$\beta_0 T_\beta = \beta_0 \left[\mathcal{T}_\beta^{(2)} + L \left(V_{\beta+}^{(1)} - \mathcal{T}^{(1)} \right) - \frac{L^2}{2} V_+^{(0)} \right], \quad (5)$$

where on the RHS we used the known decompositions of the kernel [10, 32] and the NNLO coefficient function determined in [30]:

$$V^{(1)}/C_F = \beta_0 V_\beta^{(1)} + \Delta V^{(1)}, \quad (6a)$$

$$\mathcal{T}^{(2)} = \beta_0 \mathcal{T}_\beta^{(2)} + \mathcal{T}_c^{(2)}. \quad (6b)$$

With the help of these expressions, T_{NNLO} can be recast in the more compact form

$$T_{\text{NNLO}} = C_F T_0 \otimes [\beta_0 T_\beta + T_{\Delta V} + T_L + \mathcal{T}_c^{(2)}], \quad (7)$$

where

$$T_{\Delta V} = L \Delta V_+^{(1)}, \quad (8a)$$

$$T_L = C_F L \left(\frac{L}{2} V_+^{(0)} \otimes V_+^{(0)} + \mathcal{T}^{(1)} \otimes V_+^{(0)} \right). \quad (8b)$$

It is useful to express the elements in Eqs. (4), (6), (8) in convolution form by employing the eigenfunctions $\psi_n(x)$ of the LO ERBL evolution equation. This leads to

simpler expressions, e.g., (8b) becomes (arguments suppressed)

$$T_L \otimes \psi_n = 2C_F L v(n) \left[L v(n) \psi_n + \mathcal{T}^{(1)} \otimes \psi_n \right], \quad (8c)$$

where the quantities $v(n)$ denote the eigenvalues of the ERBL evolution kernel $V_+^{(0)} \otimes \psi_n = 2v(n)\psi_n$, while the eigenfunctions ψ_n can be expressed in terms of the conformal basis of the Gegenbauer harmonics: $\psi_n(x) = 6x\bar{x}C_n^{(3/2)}(x - \bar{x})$. This representation will be further used in Sec. IV B in connection with the construction of the spectral density.

At the NNLO level we note the following. The main contribution $\beta_0 \mathcal{T}_\beta^{(2)}$ to T_{NNLO} in (7) has been calculated in [30], whereas the terms $T_{\Delta V}$ and T_L in the form they enter the corresponding contributions to the spectral density are derived here and are presented in Appendix B. Finally, the term $\mathcal{T}_c^{(2)}$ represents the still uncalculated part of T_{NNLO} .

The physics of nonperturbative interactions in the TFF is included by means of the leading-twist pion DA $\varphi_\pi^{(2)}(x, \mu_F^2)$ which is defined by the following gauge-invariant matrix element

$$\langle 0 | \bar{q}(z) \gamma_\mu \gamma_5 [z, 0] q(0) | \pi(P) \rangle |_{z^2=0} = i f_\pi P_\mu \int_0^1 dx e^{ix(z \cdot P)} \times \varphi_\pi^{(2)}(x, \mu^2), \quad (9)$$

where the lightcone gauge $A^+ = 0$ is to be imposed so that $[z, 0] = 1$, i.e., the gauge link reduces to the identity operator.

III. LIGHT-CONE SUM RULES FOR THE PION-PHOTON TFF

As mentioned in the Introduction, the existing experimental data at low Q^2 values are not precise enough to allow for reliable information extraction on the detailed behavior of the TFF in terms of magnitude and slope. This, however, would be extremely valuable given that theoretical calculations are only approximations and one needs some quantitative etalon to estimate more precisely their range of reliability that is intimately related to various perturbative and nonperturbative contributions with their own sources of uncertainties. The publication of the BESIII data may change this situation significantly. Our particular aim in this paper is to work out the applicability limits of our LCSR-based approach for the calculation of the pion-photon TFF in the low- Q^2 regime in anticipation of this set of data. To this end, let us now consider the pion-photon TFF in more detail within the method of LCSRs, which is based on the operator product expansion on the lightcone and enables the systematic computation of QCD radiative corrections and higher-twist contributions.

Within this approach, the form factor for the $\pi \rightarrow \gamma$ transition is described in terms of a dispersion integral which employs the spectral density

$$\bar{\rho}(Q^2, x) = (Q^2 + s)\rho^{\text{pert}}(Q^2, s). \quad (10)$$

The quantity $\rho^{\text{pert}}(Q^2, s)$ is given by

$$\rho^{\text{pert}}(Q^2, s) = \frac{1}{\pi} \text{Im} F_{\text{pert}}^{\gamma^* \gamma^* \pi^0}(Q^2, -s - i\varepsilon) \quad (11)$$

$$Q^2 F^{\gamma^* \gamma \pi}(Q^2) = \frac{\sqrt{2}}{3} f_\pi \left[\frac{Q^2}{m_\rho^2} \int_{x_0}^1 \exp\left(\frac{m_\rho^2 - Q^2 \bar{x}/x}{M^2}\right) \bar{\rho}(Q^2, x) \frac{dx}{x} + \int_0^{x_0} \bar{\rho}(Q^2, x) \frac{dx}{\bar{x}} \right]. \quad (12)$$

The expression on the RHS of Eq. (12) depends on various parameters and is bounded in the region $x_0 = Q^2/(Q^2 + s_0)$. In our present analysis, the Borel parameter M^2 is taken to vary in the interval $[0.7 - 1.0]$ GeV^2 as in our previous works [5, 11, 12]. But in order to estimate the uncertainty due to the variation of this parameter, we also consider the larger value $M^2 = 1.5 \text{ GeV}^2$ employed in [17, 18]. The duality interval in the vector channel is assumed to be $s_0 \simeq 1.5 \text{ GeV}^2$, whereas $m_\rho = 0.77 \text{ GeV}$ [33], and the pion decay constant has the value $f_\pi = 132 \text{ MeV}$. Expression (12) represents a sum rule which makes use of a simple δ -function *ansatz* to model the ρ -meson resonance. In the real calculation carried out here, the ρ and ω resonances are taken into account in terms of the Breit-Wigner (BW) form, as done before in [10].

The leading-twist pion DA $\varphi_\pi^{(2)}$ is expanded in terms of the eigenfunctions $\psi_n(x)$ to read

$$\varphi_\pi^{(2)}(x, \mu^2) = \psi_0(x) + \sum_{n=2,4,\dots}^\infty a_n(\mu^2) \psi_n(x) \quad (13)$$

and satisfies the normalization condition $\int_0^1 dx \varphi_\pi^{(2)}(x, \mu^2) = 1$, so that $\psi_0(x) = \varphi_\pi^{\text{asy}} = 6x\bar{x}$ is the asymptotic (asy) DA. The conformal coefficients $a_n(\mu^2)$ encode the nonperturbative information and are not calculable within pQCD. In our analysis we will consider various model DAs for the pion pertaining to different nonperturbative approaches from which these coefficients are determined. For the sake of definiteness, the numerical uncertainty estimation procedure in our analysis will be based on the set of the BMS DAs, determined in [29] using QCD sum rules with nonlocal condensates (NLC)s. This choice introduces some bias but it is not conflicting with observations [12] and does not lead to an underestimation of the size and influence of the theoretical uncertainties. Moreover, it should not be understood as the result of a priori justification of these DAs. The low- Q^2 data alone are not sufficient to draw definite conclusions about the shape of the pion

and can be calculated in fixed-order QCD perturbation theory. Then, taking into account that $s = \bar{x}Q^2/x$, the TFF assumes the following form

DA.

Turning our attention to the spectral density, we first note that each contribution of definite twist (tw) to ρ^{pert} in Eq. (11), can be obtained from the convolution of the associated hard part with the corresponding pion DA of the same twist [34] so that one gets

$$\rho^{\text{pert}}(Q^2, s) = \rho_{\text{tw-2}} + \rho_{\text{tw-4}} + \rho_{\text{tw-6}} + \dots \quad (14)$$

We then express the twist-two part of $\bar{\rho}(Q^2, x)$ as a sum over the partial spectral densities $\bar{\rho}_n$ each related to a particular harmonic ψ_n . In this way, we obtain ($a_0 = 1$)

$$\bar{\rho}(Q^2, x) = \sum_{n=0,2,4,\dots} a_n(Q^2) \bar{\rho}_n(Q^2, x) + \bar{\rho}_{\text{tw-4}}(Q^2, x) + \bar{\rho}_{\text{tw-6}}(Q^2, x), \quad (15)$$

where

$$\begin{aligned} \bar{\rho}_n(Q^2, x) &= \bar{\rho}_n^{(0)}(x) + a_s \bar{\rho}_n^{(1)}(Q^2, x) + a_s^2 \bar{\rho}_n^{(2)}(Q^2, x) + \dots, \\ \bar{\rho}_n^{(0)}(x) &= \psi_n(x); \quad a_s = a_s(Q^2). \end{aligned} \quad (16)$$

The various terms of the spectral density in (16) are the key computational ingredients in our dispersion-relation-based LCSR analysis and are therefore given explicitly in Appendix B.

The second term in Eq. (14) is the twist-four contribution to the spectral density which reads [34]

$$\bar{\rho}_{\text{tw-4}}(Q^2, x) = \frac{\delta_{\text{tw-4}}^2(Q^2)}{Q^2} x \frac{d}{dx} \varphi^{(4)}(x), \quad (17)$$

with the twist-four coupling parameter being given by $\delta_{\text{tw-4}}^2 \approx (1/2) \lambda_q^2 = (1/2) (0.4 \pm 0.05) \text{ GeV}^2$ at $Q^2 \approx 1 \text{ GeV}^2$ [31], where λ_q^2 denotes the average virtuality of vacuum quarks [35]. The full twist-four pion DA — which originates from the contributions of the two- and three-particle twist-four DAs — is approximated here by its asymptotic form [34]

$$\varphi_\pi^{(4)}(x) = \frac{80}{3} x^2 (1-x)^2, \quad (18)$$

see [17] (Sec. 3 C there) for further discussion.

The twist-six term $\bar{\rho}_{\text{tw-6}}(Q^2, x) = (Q^2 + s)\rho_{\text{tw-6}}(Q^2, s)$

in Eq. (14) was first computed in [17] (Eq. (58) there) and is given by the following expression

$$\bar{\rho}_{\text{tw-6}}(Q^2, x) = 8\pi \frac{C_F}{N_c} \frac{\alpha_s \langle \bar{q}q \rangle^2}{f_\pi^2} \frac{x}{Q^4} \left[-\left[\frac{1}{1-x} \right]_+ + (2\delta(\bar{x}) - 4x) + (3x + 2x \log x + 2x \log \bar{x}) \right], \quad (19)$$

where $\alpha_s = 0.5$ and $\langle \bar{q}q \rangle^2 = (0.242 \pm 0.01)^6 \text{ GeV}^6$ [36]. We have independently verified and confirmed this expression, which may be considered as an inverse power correction to the coefficient function. It is important to make a remark on the structure of Eq. (19) in conjunction with the diagrams in Fig. 4 in [17]: The first term in the square brackets originates from diagram (a), while the second one stems from diagram (b), and the third one derives from diagrams (c) and (d). To discuss the structure of the LCSR in Eq. (12), it is useful to do it in comparison with the pQCD factorization formula, looking more closely and critically at the behavior of the TFF in the low to intermediate Q^2 region, say, between 1 and

5 GeV^2 . As we will make more explicit below, the main effect in using the LCSR instead of the pQCD expression is the possibility of a successive inclusion into the TFF of the higher harmonics $\psi_{n>0}(x)$ as Q^2 grows. This effect can be revealed already at the level of the leading-order approximation of both expressions.

To this end, consider the contribution of a given harmonic to the expression in the square brackets in Eq. (12) and approximate the perturbative part of the spectral density by $\bar{\rho}(Q^2, x) \rightarrow \bar{\rho}_n^{(0)}(x) = \psi_n(x)$, cf. (16). This way, we obtain a physical correspondence between the LCSR on the left below

$$\begin{array}{ccc} \text{LCSR} & \Leftrightarrow & \text{pQCD,} \\ Q^2 F_n^{\text{LCSR}}(Q^2) = \frac{Q^2}{m_\rho^2} e^{\frac{m_\rho^2}{M^2}} \int_{x_0}^1 e^{-\frac{Q^2 \bar{x}}{M^2}} \psi_n(x) \frac{dx}{x} + \int_0^{x_0} \psi_n(x) \frac{dx}{\bar{x}} & \Leftrightarrow & Q^2 F_n^{\text{pQCD}}(Q^2) = \int_0^1 \psi_n(x) \frac{dx}{\bar{x}} = 3. \end{array} \quad (20)$$

and the lowest-order leading-twist contribution from pQCD, shown on the right, which amounts to the inverse moment of ψ_n on account of $6 \int_0^1 dx x C_n^{(3/2)}(x - \bar{x}) = 3$ for any n .

This correspondence can be completely vindicated by the following observations:

- For $Q^2 \gg s_0$, $x_0 = (1 + s_0/Q^2)^{-1} \rightarrow 1$ and, employing the values of m_ρ , s_0 and M^2 given farther above, the first term in the LCSR on the left, which models the hadronic content of the quasireal photon, becomes suppressed with Q^2 . Hence, the whole expression tends to the pQCD result, shown on the right of (20), establishing also a *mathematical* correspondence between the LCSR and the pQCD expression. In this latter result, all harmonic contributions of expansion (13) *appear at once* – see the horizontal uppermost line in Fig. 1.
- In the opposite kinematic region $Q^2 \lesssim s_0$, $x_0 \lesssim 1/2$, both terms on the left are of the same order of magnitude and hence the result differs strongly

from that on the right, implying that LCSRs and pQCD lead to different predictions for the TFF. This is, mainly because higher twists, contributing via the first term in the LCSR, are not accounted for in the pQCD expression. This difference ensues from the treatment (in the LCSR) of the quasireal photon by means of the vector-meson dominance model. This model has been used to construct the phenomenological spectral density and effectively takes into account long-distance gluon interactions pertaining to this photon vertex [34]. The key parameter to manage these long-distance (nonperturbative) effects is s_0 , the duality interval, and encompasses the masses of the vector-meson family m_ρ, \dots entering the first term on the left in (20).

On the other hand, the Gegenbauer harmonics are included into the TFF sequentially, i.e., term by term with increasing index n , in correspondence with the growth of Q^2 , giving rise to an oscillatory behavior. These zero crossings of the harmonics accumulate in the vicinity of 1 GeV^2 to build a knot (see Fig. 1.) The contributions stemming from different harmonics vanish near the first

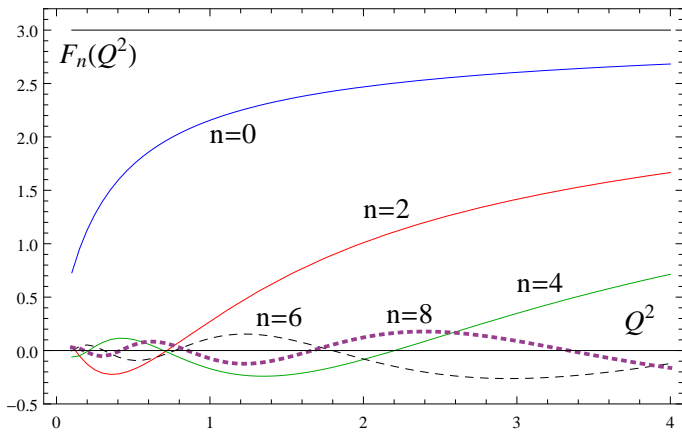


FIG. 1: Contributions of $F_n^{\text{LCSR}}(Q^2)$ to the TFF entering the left side of (20) and originating from the successive inclusion of Gegenbauer harmonics of increasing order n . The harmonics with $n = 0, 2, 4, 6, 8$ are shown explicitly using the following designations from top to bottom: $n = 0$ — upper solid blue line, $n = 2$ — middle solid red line, $n = 4$ — solid green line, $n = 6$ — dashed black line, $n = 8$ — dotted pink line. All harmonics, except ψ_0 , have a zero crossing in the vicinity of $Q^2 \approx 0.8 \text{ GeV}^2$. The topmost solid horizontal line corresponds to the F_n^{pQCD} result in (20) (right side).

knot at $Q^2 \approx 0.8 \text{ GeV}^2$, so that only the term with $n = 0$ survives which does not oscillate but grows uniformly. This leads for momentum values $Q^2 \lesssim 1.4 \text{ GeV}^2$ to the dominance of the zero harmonic (ψ_0) contribution to the TFF. At higher Q^2 values, the contributions stemming from higher harmonics, beginning with ψ_2 , succeeded by ψ_4 , and so forth, start gradually to increase. On the contrary, the suppression of higher harmonics at low momenta renders the “spectral content” of the DA $\varphi_\pi^{(2)}$ less important. The certain impact of importance and uncertainties of the different contributions will be discussed in the next section.

IV. LCSR PREDICTIONS FOR $F_{\gamma\pi}$ AND THEIR UNCERTAINTIES

In this section we identify the main sources of the various theoretical uncertainties and estimate their effects on the computation of the pion-photon TFF within the LCSR approach.

A. Leading twist DA models and their uncertainties

The key nonperturbative input in the computation of the TFF is the pion distribution amplitude of twist two, i.e., Eq. (13), which depends on the conformal coefficients $a_n(\mu^2)$. In our approach $\{a_n(\mu^2)\}$ are obtained from QCD sum rules with NLCs [29], first proposed in [35, 37]. The method in [29] allows us to extract at the

typical hadronic scale $\mu^2 \approx 1.35 \text{ GeV}^2$ (emerging naturally in the approach) a whole family of DAs. This is done by fitting the sum rules for the first ten moments

$$\langle \xi^N \rangle_\pi \equiv \int_0^1 dx (2x-1)^N \varphi_\pi^{(2)}(x, \mu^2), \quad (21)$$

where $\xi = x - \bar{x}$, together with their uncertainties. The DAs are then expressed in terms of a two-parametric model of the generic form

$$\varphi_\pi^{\text{BMS}}(x, \mu^2) = 6x\bar{x} \left[1 + a_2 C_2^{(3/2)}(\xi) + a_4 C_4^{(3/2)}(\xi) \right]. \quad (22)$$

This parametrization is defacto justified because all higher conformal coefficients $a_n(\mu^2)$ were found by calculating the moments $\langle \xi^N \rangle_\pi$ ($N = 2, 4, \dots, 10$) to be negligible but bearing a large margin for error, see [29, 38] for details. The admissible region of the first two moments $\langle \xi^2 \rangle_\pi$ and $\langle \xi^4 \rangle_\pi$ is shown graphically in Fig. 2 in the form of an upward pointing slanted (green) rectangle, with its center being marked by the symbol \mathbf{X} and denoting the BMS DA [29]. The associated pairs of (a_2, a_4) values fit

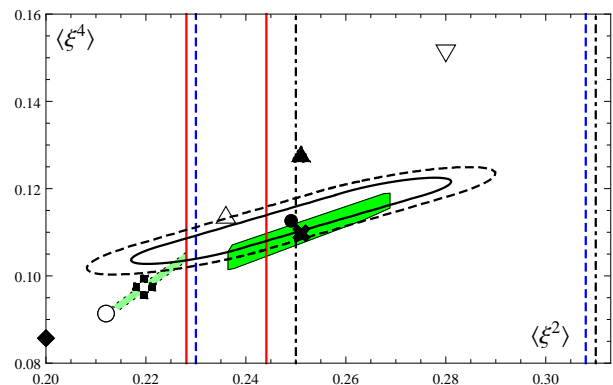


FIG. 2: Locations of various pion DAs projected onto the plane spanned by the moments $\langle \xi^2 \rangle$ and $\langle \xi^4 \rangle$ at the momentum scale $\mu = 2 \text{ GeV}$. For those DAs which were originally determined at a lower normalization scale, NLO evolution has been employed. Upward pointing stretched green rectangle — BMS admissible region with $\lambda_q^2 = 0.4 \text{ GeV}^2$, including the BMS DA \mathbf{X} ; $\mathbf{+}$ — platykurtic DA [21] within the admissible region of similar DAs determined in [22] with $\lambda_q^2 = 0.45 \text{ GeV}^2$; \circ — Light-Front DA [39]; \blacklozenge — asymptotic DA; \blacktriangle — DSE-DB π DA [20]; \blacktriangledown — DSE-RL π DA [20]; \triangleleft — AdS/QCD π DA [13]. The vertical lines denote the constraints extracted for $\langle \xi^2 \rangle$ from various lattice simulations: solid red lines — [40]; dashed blue lines — [41]; dashed-dotted lines — [42]. 1σ (solid line) and 2σ (dashed line) error ellipses obtained with a LCSR-based fit to the CELLO [23], CLEO [24], BABAR ($\leq 9 \text{ GeV}^2$) [1], and Belle [4] data.

best all moments $\langle \xi^N \rangle$ with $N = 2, 4, \dots, 10$ within the estimated errors. These moments were determined by employing the nonlocality parameter $\lambda_q^2 = 0.4 \text{ GeV}^2$.

One can compute the values of the moments and the conformal coefficients at any desired momentum scale using the ERBL evolution equation. The symbol $\mathbf{+}$

in this figure denotes the position of the recently proposed [21] platykurtic (pk) pion DA, obtained within the BMS approach but using the still admissible value $\lambda_q^2 = 0.45 \text{ GeV}^2$. A whole region of such platykurtic DAs was determined subsequently by two of us in [22] and is shown in this figure in terms of the shorter rectangle in light-green color on the left of the previous one. It is worth mentioning that the platykurtic DA is a unimodal curve with a flat peak at $x = 1/2$ and suppressed tails at $x = 0, 1$. The numerical values of the second and fourth moments of these two sets of DAs have been calculated at the momentum scale $\mu = 2 \text{ GeV}$ after NLO evolution using the $\overline{\text{MS}}$ scheme to obtain

$$\times \langle \xi^2 \rangle^{\text{BMS}} = 0.251_{-0.015}^{+0.018}, \langle \xi^4 \rangle^{\text{BMS}} = 0.110_{-0.008}^{+0.009}; \quad (23)$$

$$\clubsuit \langle \xi^2 \rangle^{\text{pk}} = 0.220_{-0.006}^{+0.009}, \langle \xi^4 \rangle^{\text{pk}} = 0.098_{-0.005}^{+0.008}. \quad (24)$$

The corresponding conformal coefficients are given by

$$a_2^{\text{BMS}} = 0.149_{-0.043}^{+0.052}, a_4^{\text{BMS}} = -0.096_{-0.058}^{+0.063}; \quad (25)$$

$$a_2^{\text{pk}} = 0.057_{-0.019}^{+0.024}, a_4^{\text{pk}} = -0.013_{-0.019}^{+0.022}. \quad (26)$$

Note that the numerical values provided above for the moments of the BMS DA are slightly different from those quoted in Table 1 of [22]. The reason for this discrepancy is that here we use a more advanced code for the NLO evolution than that employed in [43] and quoted in [22]. The new code takes into account the quark-mass thresholds in more accurate way and yields less suppression due to evolution. We present these results at the momentum scale $\mu = 2 \text{ GeV}$ because this scale is commonly used in lattice calculations of $\langle \xi^2 \rangle$ and a_2 , as those indicated in the figure by the vertical lines. The solid red lines furthest to the left display the most recent constraints determined in [40], while the dashed blue lines show the older results of the same group [41], and the dashed-dotted lines reproduce the regions of values computed in [42]. The corresponding numerical values of the second moment, in the same order of appearance, are

$$\langle \xi^2 \rangle = 0.2361(41)(39) \quad [40] \quad (27a)$$

$$\langle \xi^2 \rangle = 0.269(39) \quad [41] \quad (27b)$$

$$\langle \xi^2 \rangle = 0.28(2)(1) \quad [42]. \quad (27c)$$

Note that the total error shown in Fig. 2 with reference to Eq. (27a) is the linear sum of the errors in parentheses. Assuming instead that these errors are statistically independent and obey normal distributions, we would obtain by the sum in quadrature a somewhat narrower range of constraints on $\langle \xi^2 \rangle$ than the vertical solid (red) lines. A detailed treatment of the extraction of the conformal coefficients from these lattice constraints is given in [11, 22, 43]. On the other hand, the symbol \bigcirc denotes the model DA from [39] extracted within a light-front-based framework. This DA has a single broad peak and suppressed tails like the platykurtic DA.

In Fig. 2 the asymptotic DA is also shown in terms of the symbol \blacklozenge , while \blacktriangle and \blacktriangledown represent, respectively, the

DSE-DB and DSE-RL π DAs [20], where the abbreviations are labels for the most advanced kernel — DB — and the rainbow ladder (RL) approximation in the use of Dyson-Schwinger equations (DSE) — [15]. In this figure, we also include the LCSR-based (cf. Eq. (12)) 1σ (solid black line) and 2σ (dashed black line) error regions of the CELLO [23], CLEO [24], and Belle [4] data in terms of two parameters, viz., $\langle \xi^2 \rangle$ and $\langle \xi^4 \rangle$. The BABAR [1] data below $Q^2 \leq 9 \text{ GeV}^2$ have also been taken into account. One observes that there is a sizeable overlap between the BMS region of bimodal DAs (larger green strip) and the data. This overlap is also compatible with the lattice constraints. The platykurtic region has a small overlap with the 1σ and 2σ error ellipses, being at the same time just on the lower boundaries of the lattice constraints on $\langle \xi^2 \rangle$. On the other hand, the broad, endpoint-enhanced DSE DAs (\blacktriangle and \blacktriangledown) conform within errors with the older lattice constraints but disagree with the data up to the level of 2σ . It is fair to notice here that the authors of [15] argue that their predictions for $Q^2 F_{\gamma\pi}(Q^2)$, computed with a QCD-based framework in terms of Dyson-Schwinger equations, agree with the CELLO, CLEO, and Belle sets of data and thus belong to the green band of predictions described in [12]. However, the truncation scheme in this approach cannot systematically connect Eq. (2) with the twist expansion. The incompatibility between these DSE-based results and our findings in Fig. 2, obtained with a LCSR-based data fit, demands further examination.

A similarly broad pion DA $(8/\pi)\sqrt{x\bar{x}}$, based on the AdS/QCD and light-front holography, is displayed in this figure by the symbol \triangle [13]. This DA appears to be just inside the upper boundary of the 2σ error ellipse of the experimental data. The predictions for $Q^2 F_{\gamma\pi}(Q^2)$ obtained with this pion DA were found [13, 14] to agree well with the CELLO and CLEO data, but to disagree with BABAR's large Q^2 data. They belong to the green band of theoretical predictions in the classification scheme of Ref. [12] (see Fig. 2 there) and conform with the Belle data as well. As a final remark, we note that a faithful conformal expansion of such broad DAs, like the DSE DAs and the holographic one, should include a much larger number of terms of the order of 50. Thus, the projection on the $(\langle \xi^2 \rangle, \langle \xi^4 \rangle)$ plane in Fig. 2 is a rather crude approximation for such DAs, see [22, 43] for further discussion.

B. Higher-order radiative corrections

In this subsection we discuss the uncertainties entailed by the NNLO radiative corrections, entering the spectral density in (16). To start with, recall Eq. (7) in conjunction with the equations in (5) and (8). To continue, we reduce the full spectral density $\bar{\rho}^{(2)}$ to the expression $a_s^2 \bar{\rho}_n^{(2)}(Q^2, x) \rightarrow a_s^2 \beta_0 \bar{\rho}_n^{(2\beta)}(Q^2, x)$, cf. Eq. (5), ignoring this way all other terms in Eq. (7). This β_0 part of the spectral density is given in Appendix B and has already

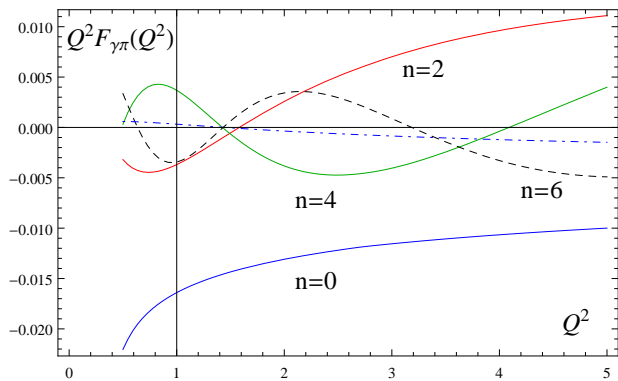


FIG. 3: Partial contributions $F_n^{\text{NNLO}}(Q^2)$ to the TFF originating from the NNLO- β_0 term. Only the results for the first Gegenbauer harmonics with $n = 0, 2, 4, 6$ are shown using the same notations as in Fig. 1. The additional dashed-dotted (light-blue) flat line represents the zero-harmonic contribution related to the NNLO - ΔV term.

been used to obtain the NNLO contribution to the TFF within the LCSR framework, see [5, 10, 21, 44, 45]. It turns out that this contribution is negative with a magnitude of the order of 0.01 GeV to be compared with 0.1 GeV of the total magnitude of the TFF at the generic hadronic boundary $Q^2 = 1 \text{ GeV}^2$ of the pQCD applicability. To increase the accuracy of the LCSR, we improve the treatment of the NNLO contribution by taking into account in the spectral density further terms related to expressions (8a) and (8b) of the hard-scattering amplitude. This is a novelty of the present work and allows us fuller treatment of the NNLO contribution and finer analysis of its uncertainties.

The uncertainty of the NNLO coefficient function $\mathcal{T}^{(2)} = \beta_0 \mathcal{T}_\beta^{(2)} + \mathcal{T}_c^{(2)}$ is induced by the yet uncalculated term $\mathcal{T}_c^{(2)}$, whereas all other elements in T_{NNLO} given by Eq. (7) are now known. Lacking knowledge of the complete structure of the NNLO term, it seems prudent to assume that the missing term $\mathcal{T}_c^{(2)}$ may have a comparable magnitude as $\beta_0 \mathcal{T}_\beta^{(2)}$ which in turn implies that the supposed uncertainty ensuing from our approximate treatment will be rather overestimated. In any case, each term in expression (7) for the T_{NNLO} hard-scattering amplitude entails an associated contribution to the spectral density $\bar{\rho}_n^{(2)}$, notably,

$$\bar{\rho}_n^{(2)} = C_F \left(\beta_0 \bar{\rho}^{(2\beta)} + \bar{\rho}^{(2\Delta V)} + \bar{\rho}^{(2L)} + \mathcal{T}_c^{(2)} \right)_n. \quad (28)$$

Here $\bar{\rho}^{(2\beta)}$, $\bar{\rho}^{(2\Delta V)}$, and $\bar{\rho}^{(2L)}$ stem from Eqs. (5), (8a), and (8b), respectively, so that

$$\bar{\rho}_n^{(2k)} = C_F^{-1} \text{Im} (T_0 \otimes T_k \otimes \psi_n) \quad (k = \beta, \Delta V, L), \quad (29)$$

while the term $\mathcal{T}_c^{(2)}$ enters autonomously as in (7). According to our conjecture above, we will replace the unknown term $\mathcal{T}_c^{(2)}$ by $\pm \beta_0 \mathcal{T}_\beta^{(2)}$ inducing this way the discussed uncertainty $\Delta \bar{\rho}_n^{(2)} = \pm \beta_0 \bar{\rho}^{(2\beta)}$ in the spectral density $\bar{\rho}_n^{(2)}$. The final effect of these uncertainties on the TFF in the low-mid Q^2 region will be addressed later in Sec. V.

To clarify the role of the partial NNLO radiative corrections, we present in Fig. 3 the NNLO- β_0 contribution to the TFF, i.e., F_n^{NNLO} , for the first few terms up to $n = 6$ of the Gegenbauer-harmonics expansion in comparison with the NNLO- ΔV contribution for the zero harmonic. Taking into account that the NNLO- L contribution is equal to zero for the zero harmonic, we conclude from this figure that the additional NNLO- L - and NNLO- ΔV terms can be safely ignored.

The main (negative in sign) contribution is provided by the ψ_0 -harmonic and is denoted by the lowest solid (blue) curve in Fig. 3. The higher harmonic contributions are smaller than this and oscillate. Remarkably, they become positive but with a small delay in Q^2 relative to the LO case shown in Fig. 1. Also the first knot is slightly shifted to the right and appears at $\sim 1.4 \text{ GeV}^2$. The explicit expressions for the elements of $\bar{\rho}_n^{(1)}$ and $\bar{\rho}_n^{(2)}$ are outlined in Appendix B.

V. NUMERICAL RESULTS FOR $F_{\gamma\pi}$ IN THE LOW- Q^2 SPACELIKE DOMAIN

Let us now discuss our LCSR-based calculation of the TFF in terms of Fig. 4 which effects graphically our core predictions together with their various theoretical uncertainties worked out in the previous section. This analysis is bounded from below by the applicability limit of the pQCD approach at the generic hadronic scale 1 GeV^2 which we indicated in this figure by a vertical line. Although the obtained predictions are mathematically correct also below this boundary, one cannot estimate their reliability from the physical point of view. Therefore, the displayed predictions below 1 GeV^2 only serve to indicate the possible trend of the TFF in this momentum region. The proper exploitation of the low-energy domain would demand additional means, e.g., use of the axial anomaly exploited in [46–48] and recently connected to the LCSRs in [49].

The considered uncertainties illustrated in Fig. 4 include (i) the range of the admissible Gegenbauer con-

formal coefficients a_2 and a_4 for the BMS DAs deter-

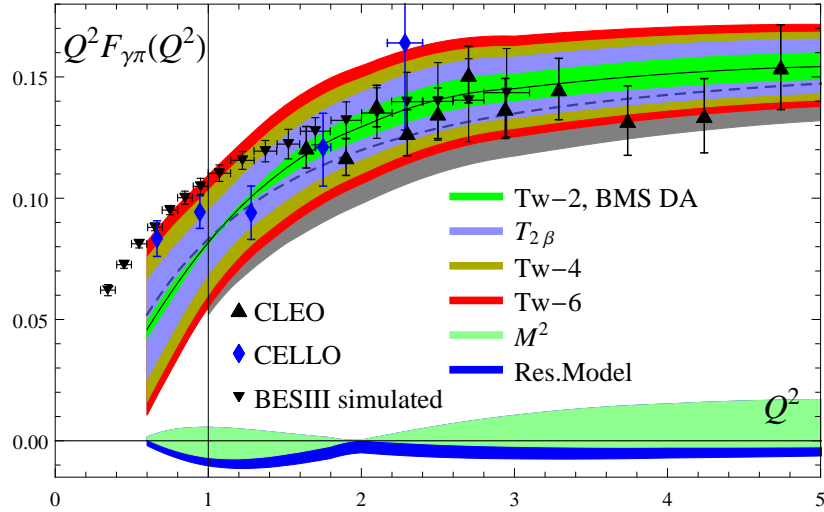


FIG. 4: Upgraded LCSR calculation of the pion-photon TFF using as nonperturbative input the twist-two pion DAs obtained in [29] with $\lambda_q^2 = 0.40 \text{ GeV}^2$ and taking into account NLO ERBL evolution. The central wide (green) strip represents the result obtained with the whole family of the BMS pion DAs, varying the conformal coefficients (a_2, a_4) within the appropriate region cf. (26) which corresponds to the slanted (green) rectangle in the plane spanned by the associated moments $\langle \xi^2 \rangle^{\text{BMS}}, \langle \xi^4 \rangle^{\text{BMS}}$ in Fig. 2. The central line inside the green strip shows the result for the BMS model. The uncertainties ensuing from different contributions are identified in the graphics and are discussed in the text. Taking into account the NNLO uncertainties gives rise to the violet band next to the central green strip, whereas the variation of the twist-four (Tw-4) and the twist-six (Tw-6) parameters generates (from the inside to the outside) the orange and red outer strips, respectively. The two bands at the bottom of the figure show the additional uncertainties originating from the variation of the Borel parameter in the interval $M^2 \in [0.7 - 1.5] \text{ GeV}^2$ (wide light-green band) and the dependence on the modeling of the effective pion resonance in the LCSR narrow blue strip), the latter being estimated as the difference of the results obtained by using the BW model vs. the δ -function resonance model for the ρ and ω resonances. These two uncertainties have to be added to the “rainbow” band shown on the top of the figure. We also show in the graphics the influence of a non-vanishing small virtuality of the quasireal photon in terms of the light-grey strip below all others (see text for explanations). The thick dashed line (close to the BMS solid line) corresponds to the platykurtic model [21, 22] and serves as a rough measure of the uncertainty induced by using $\lambda_q^2 = 0.45 \text{ GeV}^2$ inside the BMS approach. The vertical line at 1 GeV^2 marks the typical applicability boundary of our framework below which its reliability may become questionable.

mined via QCD sum rules with nonlocal condensates and using the nonlocality parameter $\lambda_q^2 = 0.40(5) \text{ GeV}^2$ [29] (narrow central green strip), (ii) the result obtained by employing the platykurtic DAs derived with the same method but with the slightly larger virtuality $\lambda_q^2 = 0.45 \text{ GeV}^2$ [21] (thick dashed line slightly below the central strip), (iii) the effect attributed to the unknown term $\mathcal{T}_c^{(2)}$ in the NNLO contribution that has been approximated by $\pm \beta_0 \mathcal{T}_\beta^{(2)}$ (wide violet bands just above and below the central green strip), (iv) the variation of the twist-four parameter $\delta^2 = 0.19 \pm 0.038 \text{ GeV}^2$ in the range $\delta^2 \in [0.152 - 0.228] \text{ GeV}^2$ (light brown strips above and below the previous ones), (v) the errors induced by the variation of the pre-factor $(1_{-0.23}^{+0.28}) \langle \sqrt{\alpha_s} \bar{q}q \rangle^2$ related to the uncertainty of the value of the quark condensate in front of the twist-six expression in (19) (red strips on the boundaries), (vi) the effect of a small but finite virtuality of the quasireal photon (strip in grey color below all the others) — to be discussed separately below, (vii) the ambiguities in selecting the auxiliary Borel parameter $M^2 \in [0.7 - 1.5] \text{ GeV}^2$ (green band narrowing at 2 GeV^2 at the bottom), (viii) the influence of the phenomenological description of the resonance in the LCSR (narrow

TABLE I: Sources and percentage estimates at $Q^2 = 3 \text{ GeV}^2$ of the systematic theoretical uncertainties in the LCSR-based calculation of the pion-photon TFF illustrated in Fig. 4.

Source	Uncertainty (%)
Unknown NNLO term $\mathcal{T}_c^{(2)}$	∓ 4.8
Range of Tw-2 BMS DAs	$-3.4 \div 4.1$
Tw-4 coupling $\delta^2 = [0.152 - 0.228] \text{ GeV}^2$	± 3.0
Tw-6 parameter variation	$-2.4 \div 3.0$
Total	$-13.6 \div 14.9$
Borel parameter $M^2 \in [0.7 - 1.5] \text{ GeV}^2$	$-1.6 \div 7.2$
Resonance description δ vs. BW	$-3.6 \div 0$
Small virtuality of quasireal photon	$-5.4 \div 0$

blue strip at the bottom) which displays the difference between the results obtained from the Breit-Wigner and the δ -function resonance models. These sources of systematic uncertainties have been collected for convenience in Table I together with their partial uncertainties (%) at $Q^2 = 3 \text{ GeV}^2$.

Focusing attention on the TFF in the vicinity of 1 GeV^2 , we recall our discussion of the correspondence of the two sides of Eq. (20) to notice that in this momentum region mainly the ψ_0 -harmonic contributes, as illustrated in Fig. 1. This makes it evident that the contributions from different harmonics in the vicinity of the knot at $Q^2 \sim 1 \text{ GeV}^2$ vanish.

A possible small virtuality q^2 of the quasireal photon affects the TFF and leads to an additional uncertainty of the predictions which however is not universal but has to be estimated for each specific experiment. Theoretically, this effect can be expressed in terms of the susceptibility $\Delta(Q^2)$ (linear response) which was invented in [5] (Sec. III there). One has

$$\begin{aligned} \tilde{F}(Q^2, q^2) &\approx F(Q^2) [1 + \Delta(Q^2)q^2] , \\ \Delta(Q^2) &\equiv \frac{\tilde{F}'_{q^2}(Q^2, q^2 = 0)}{F(Q^2)} . \end{aligned} \quad (30)$$

The susceptibility for the considered interval of Q^2 in Fig. 4 is approximately $\Delta(Q^2) \simeq -1 \text{ GeV}^{-2}$ as one can see from Fig. 3 in [5]. To get a qualitative estimate of this uncertainty and its influence on the TFF, we use $q^2 \approx 0.04 \text{ GeV}^2$, which represents the maximal virtuality of the quasireal photon allowed in the Belle experiment [5]. The result of the calculation is illustrated in Fig. 4 in terms of the lowest (grey) strip and has the tendency to reduce the magnitude of the form factor in the whole range of Q^2 up to asymptotic values, see [5].

Thus, from Fig. 4 and Table I one may conclude that for a given DA, the largest uncertainties in the low-to-mid $Q^2 \in [1 - 5] \text{ GeV}^2$ range originate from the NNLO radiative correction and the twist-four and twist-six contributions.

VI. CONCLUSIONS

The work presented here constitutes a systematic analysis of the theoretical uncertainties entering the calculation of the pion-photon transition form factor within the framework of LCSRs. This method represents a very effective theoretical tool for the study of this pion observable because it enables the sequential inclusion of various contributions with controlled theoretical accuracy. To be specific, we estimated the following main uncertainties: (i) the relevance of the NNLO radiative corrections, (ii) the ambiguity induced by the still unknown NNLO term $\mathcal{T}_c^{(2)}$, (iii) the influence of the twist-four and twist-six terms, (iv) the sensitivity of the results on auxiliary parameters, like the Borel scale M^2 , and (v) the role of

the phenomenological description of resonances by using a Breit-Wigner parametrization instead of a δ -function *ansatz*. Moreover, we computed the generic uncertainty pertaining to a small but finite virtuality of the quasireal photon, albeit the precise magnitude of this effect depends on the particular experimental setup. A full list of the considered uncertainties and the estimation of their size in percentage is given in Table I while a visualization of these contributions to the scaled TFF is provided in Fig. 4, focusing attention to the low-mid Q^2 region, where the BESIII Collaboration is expected to publish high-statistics data in the near future. The presented analysis complements and upgrades our previous works in [5, 11, 12], in which our interest was primarily concentrated on the high- Q^2 regime. On the theoretical side, our study further extends the knowledge of the NNLO contributions to the hard-scattering amplitude by computing the terms $T_{\Delta V}$ and T_L in Eq. (7). Moreover, we independently reproduced term-by-term all contributions to the twist-six correction (19), originally computed in [17], and confirmed their validity.

Acknowledgments

We thank Nils Offen and Maksym Deliyergiyev for useful discussions and comments. This work was partially supported by the Heisenberg–Landau Program (Grants 2015 and 2016), the Russian Foundation for Basic Research under Grants No. 14-01-00647 and No. 15-52-04023, and the JINR-BelRFFR grant F16D-004. A.V.P. was supported by the Chinese Academy of Sciences President’s International Fellowship Initiative (Grant No. 2016PM053), the Major State Basic Research Development Program in China (Grant No. 2015CB856903), and the National Natural Science Foundation of China (Grants No. 11575254 and No. 11175215).

Appendix A: NLO evolution kernel and coefficient functions

In this appendix, the explicit expressions for the one- and two-loop kernels of the ERBL evolution equation will be supplied, supplemented by the coefficient functions. We start by displaying the NLO evolution kernel $V^{(1)}/C_F = \beta_0 V_\beta^{(1)} + \Delta V^{(1)}$ in Eq. (6a), which has been computed in [50, 51]. In order to reveal the origin of its individual contributions, we employ the following new decomposition

$$V_+^{(1)} = C_F \left\{ \left[\beta_0 V_{\beta+}^{(1)} - C_F \dot{V}_+^{(0)} \otimes V_+^{(0)} - C_F [g_+, \otimes V_+^{(0)}] \right] + \left[-4 \left(C_F - \frac{C_A}{2} \right) \left(\frac{2}{3} V^{(0)} + 2V^a + H \right)_+ + C_F U_+ \right] \right\} \quad (A1)$$

and discuss its structure term-by-term. The first term, proportional to β_0 , has the explicit form

$$V_{\beta+}^{(1)} = \left(\dot{V}^{(0)} + \frac{5}{3} V^{(0)} + 2V^a \right)_+ \quad (A2)$$

and is related to the one-loop renormalization of α_s [10, 32]. The second term $-C_F^2 \dot{V}_+^{(0)} \otimes V_+^{(0)}$ results from

the two-loop renormalization of the composite operator [32] and can be expressed as a convolution of one-loop elements

$$\begin{aligned} \dot{V}_+^{(0)} \otimes V_+^{(0)}(x, y) = 2\mathcal{C}\theta(y > x) & \left\{ (F - \bar{F}) \left[\ln(y) \ln(\bar{y}) - \text{Li}_2(x) + \text{Li}_2(y) + \frac{\pi^2}{6} \right] \right. \\ & + \bar{F} \left[\text{Li}_2 \left(1 - \frac{x}{y} \right) - \text{Li}_2 \left(1 - \frac{\bar{x}}{\bar{y}} \right) + \ln(\bar{x}) \ln(xy) - \ln(y-x) \ln \left(\frac{\bar{x}}{\bar{y}} \right) - \frac{1}{2} \ln^2(\bar{y}) \right] \\ & + F \left[\frac{3}{2} \ln \left(\frac{x}{y} \right) + \ln \left(\frac{x}{y} \right) \ln(y-x) - \frac{1}{2} \ln^2(x) \right] - \frac{11}{4} F + 2V^b \\ & \left. + \frac{x\bar{x} (\ln^2(\bar{x}) - 2\ln(x) \ln(y) + \ln^2(y))}{y\bar{y}(x-y)} - 2 \left[\frac{x \ln(y)}{\bar{y}} + \frac{\bar{x} \ln(\bar{x})}{y} \right] \right\}, \end{aligned} \quad (A3)$$

where $F(x, y) = \frac{x}{y} \left(1 + \frac{1}{y-x} \right)$ with $\bar{F} = F(\bar{x}, \bar{y})$. Next we show the kernels $V^{(0)}$ and $\dot{V}^{(0)}$ in explicit form

$$V_+^{(0)}(x, y) = 2 \left[\mathcal{C}\theta(y > x) \frac{x}{y} \left(1 + \frac{1}{y-x} \right) \right]_+ \equiv 2 [V^a(x, y) + V^b(x, y)]_+, \quad (A4a)$$

$$\dot{V}_+^{(0)}(x, y) = 2 \left[\mathcal{C}\theta(y > x) \frac{x}{y} \left(1 + \frac{1}{y-x} \right) \ln \left(\frac{x}{y} \right) \right]_+, \quad (A4b)$$

where

$$V^a(x, y) = \mathcal{C}\theta(y > x) \frac{x}{y}, \quad V^b(x, y) = \mathcal{C}\theta(y > x) \frac{x}{y} \left(\frac{1}{y-x} \right), \quad (A4c)$$

and the symbol \mathcal{C} means $\mathcal{C} = \mathbb{1} + \{x \rightarrow \bar{x}, y \rightarrow \bar{y}\}$.

52], contains the element

Finally, the commutator $[g_+, \otimes V_+^{(0)}]$ in (A1), which gives rise to the breaking of the conformal symmetry [30,

$$g_+(x, y) = -2 \left[\theta(y > x) \frac{\ln(1-x/y)}{y-x} + \theta(y < x) \frac{\ln(1-\bar{x}/\bar{y})}{x-y} \right]_+, \quad (A5)$$

so that with (A4a) we obtain

$$\begin{aligned}
\left[g_+, \otimes V_+^{(0)} \right] (x, y) = & -2\mathcal{C}\theta(y > x) \left\{ (F - \bar{F}) (\text{Li}_2(y) - \text{Li}_2(x)) \right. \\
& + \bar{F} \left[\text{Li}_2 \left(1 - \frac{x}{y} \right) - \text{Li}_2 \left(1 - \frac{\bar{x}}{\bar{y}} \right) + \ln \left(1 - \frac{x}{y} \right) \ln \left(\frac{x\bar{y}}{y\bar{x}} \right) + \frac{1}{2} \ln \left(\frac{\bar{x}}{\bar{y}} \right) \ln(\bar{x}\bar{y}) \right] \\
& + \frac{1}{2} F \left[\ln \left(\frac{x}{y} \right) \ln \left(\frac{x\bar{y}}{\bar{x}y} \right) - \ln(xy) \ln \left(\frac{\bar{x}}{\bar{y}} \right) \right] - \frac{\pi^2}{6} (F + \bar{F}) \\
& \left. - \frac{2}{y\bar{y}} (\bar{x} \ln(\bar{x}) - (y - x) \ln(y - x) + y \ln(y)) \right\}. \tag{A6}
\end{aligned}$$

To complete the structure of the NLO evolution kernel $V_+^{(1)}$ entering Eq. (6a), we also provide the expression for $\Delta V^{(1)}$:

$$\begin{aligned}
\Delta V_+^{(1)} &= \frac{1}{C_F} V_+^{(1)} - \beta_0 V_{\beta+}^{(1)} \\
&= -C_F \dot{V}_+^{(0)} \otimes V_+^{(0)} - C_F \left[g_+, \otimes V_+^{(0)} \right] - 4 \left(C_F - \frac{C_A}{2} \right) \left(\frac{2}{3} V^{(0)} + 2V^a + H \right)_+ + C_F U_+. \tag{A7}
\end{aligned}$$

Note that the leading-order coefficient of the β function used in the above equations is

$$\beta_0 = \frac{11}{3} C_A - \frac{4}{3} T_R N_f, \tag{A8}$$

with N_f being the number of active flavors ($N_f = 4$ here) and $T_R = 1/2$, $C_F = 4/3$, $C_A = 3$ for $SU(3)_c$.

The elements collected in the second square bracket in (A1) are all diagonal with respect to the one-loop eigen-

functions ψ_n by virtue of the symmetries $U(x, y)y\bar{y} = x\bar{x}U(y, x)$ and $H(x, y)y\bar{y} = x\bar{x}H(y, x)$. These quantities are displayed below for the convenience of the reader. Note that the function $H(x, y)$ has been computed before, e.g., [32], while the function $U(x, y)$ was derived here.

$$\begin{aligned}
H(x, y) = & \mathcal{C} \left\{ \theta(x > \bar{y}) \left[2(F - \bar{F}) \text{Li}_2(1 - x/y) - 2F \ln(x) \ln(y) + (F - \bar{F}) \ln^2(y) \right] \right. \\
& + 2F \text{Li}_2(\bar{y}) [\theta(x > \bar{y}) - \theta(y > x)] + \theta(y > x) 2\bar{F} \ln(y) \ln(\bar{x}) \\
& \left. - 2F \text{Li}_2(x) [\theta(x > \bar{y}) - \theta(x > y)] \right\}, \tag{A9}
\end{aligned}$$

$$\begin{aligned}
U(x, y) = & -\frac{5}{6} V^{(0)} + 8V^a - \mathcal{C}\theta(y > x) \left[4 \frac{(y - x)}{y\bar{y}} \ln(y - x) \right] \\
& + \mathcal{C}\theta(y > x) \left[2 \frac{\bar{x}}{\bar{y}} \left(\frac{3y - 1}{y} \ln(\bar{x}) + 2 \ln(y) \right) - 2 \frac{x}{\bar{y}} \ln(y) \right]. \tag{A10}
\end{aligned}$$

Finally, the coefficient functions of the partonic subprocess, described by $\mathcal{T}^{(1)}$ and $\mathcal{T}_\beta^{(2)}$ in Eqs. (4), (5) are

$$\mathcal{T}^{(1)}(x, y) = [-3V^b + g](x, y)_+ - 3\delta(x - y), \quad (\text{A11})$$

$$\mathcal{T}_\beta^{(2)}(x, y) = \left[\frac{29}{12}2V^a + 2\dot{V}^a - \frac{209}{36}V^{(0)} - \frac{7}{3}\dot{V}^{(0)} - \frac{1}{4}\ddot{V}^{(0)} + \frac{19}{6}g + \dot{g} \right]_+ (x, y) - 6\delta(x - y). \quad (\text{A12})$$

The elements on the RHS of these equations were originally derived in [30], but are presented here in a different notation following [10], where also the omitted elements $\ddot{V}^{(0)}$ and \dot{g} can be found.

(0) — LO term $\bar{\rho}_n^{(0)}$, (1) — NLO term $\bar{\rho}_n^{(1)}$, and (2...) NNLO terms, where the dots ... indicate particular contributions pertaining to the set of equations in (4). For the default scale setting $\mu_R^2 = \mu_F^2 = Q^2$, they read

Appendix B: Elements of the spectral density $\bar{\rho}$

Here we provide the contributions to the spectral density entering Eq. (16). They are identified by the labels

$$\bar{\rho}_n^{(0)}(x) = \psi_n(x), \quad (\text{B1})$$

$$\begin{aligned} \bar{\rho}_n^{(1)}(Q^2 = \mu_F^2; x) \frac{1}{C_F} = & \left[-3(1 + v^b(n)) + \frac{\pi^2}{3} + 2v(n) \ln\left(\frac{\bar{x}}{x}\right) - \ln^2\left(\frac{\bar{x}}{x}\right) \right] \psi_n(x) \\ & - 2 \left[\sum_{l=0,2,\dots}^n G_{nl} \psi_l(x) + v(n) \left(\sum_{l=0,1,\dots}^n b_{nl} \psi_l(x) - 3\bar{x} \right) \right], \end{aligned} \quad (\text{B2})$$

$$v^b(n) = 2(\psi(2) - \psi(2+n)); \quad v(n) = 1/(n+1)(n+2) - 1/2 + 2(\psi(2) - \psi(2+n)). \quad (\text{B3})$$

The complete expression for $\bar{\rho}_n^{(1)}$ in Eq. (B2) was obtained in [10] and the content of the second square bracket was later corrected in [17] in the form it appears here. The quantities $v^b(n)$ and $v(n)$ are the eigenvalues of the elements V_+^b and $V_+^a + V_+^b$ of the one-loop kernel in Eq.

(A4a), respectively. Expressions G_{nl} and b_{nl} denote the elements of calculable triangular matrices (omitted here) — see [10, 17]. On the other hand, the β_0 , ΔV , and L parts of the NNLO spectral density have the following form

$$\begin{aligned} \bar{\rho}_n^{(2\beta)}(Q^2; x) = & \mathcal{T}_\beta^{(2)}(x, y) \otimes \psi_n(y) + \ln\left(\frac{\bar{x}}{x}\right) C_{1,n}(x) + C_{2,n}(x) - \\ & v(n) \left\{ \left[\ln^2\left(\frac{\bar{x}}{x}\right) - \frac{\pi^2}{3} \right] \psi_n(x) + 2 \ln(x) C_{3,n}(x) - 2C_{4,n}(x) \right\}, \end{aligned} \quad (\text{B4})$$

$$\bar{\rho}_n^{(2\Delta V)}(Q^2; x) = \ln\left(\frac{\bar{x}}{x}\right) \bar{C}_{1,n}(x) + \bar{C}_{2,n}(x), \quad (\text{B5})$$

$$\begin{aligned} \bar{\rho}_n^{(2L)}(Q^2; x) = & \ln\left(\frac{\bar{x}}{x}\right) \tilde{C}_{1,n}(x) + \tilde{C}_{2,n}(x) + 2C_F v^2(n) \\ & \times \left\{ \left[\ln^2\left(\frac{x}{\bar{x}}\right) - \frac{\pi^2}{3} \right] \psi_n(x) + 2 \ln(x) C_{3,n}(x) - 2C_{4,n}(x) \right\}, \end{aligned} \quad (\text{B6})$$

where we have introduced the auxiliary functions

$$C_{1,n}(x) = (V_{\beta+}^{(1)}(x, y) - \mathcal{T}_1(x, y)) \otimes \psi_n(y), \quad (\text{B7a})$$

$$C_{2,n}(x) = - \int_0^{\bar{x}} du \frac{C_{1,n}(u) - C_{1,n}(\bar{x})}{u - \bar{x}}, \quad (\text{B7b})$$

$$C_{3,n}(x) = \int_0^{\bar{x}} du \frac{\psi_n(u) - \psi_n(\bar{x})}{u - \bar{x}}, \quad (\text{B7c})$$

$$C_{4,n}(x) = \int_0^{\bar{x}} du \frac{\psi_n(u) - \psi_n(\bar{x})}{u - \bar{x}} \ln(\bar{x} - u), \quad (\text{B7d})$$

$$\bar{C}_{1,n}(x) = \Delta V_+^{(1)}(x, y) \otimes \psi_n(y), \quad (\text{B7e})$$

$$\bar{C}_{2,n}(x) = - \int_0^{\bar{x}} du \frac{\bar{C}_{1,n}(u) - \bar{C}_{1,n}(\bar{x})}{u - \bar{x}}, \quad (\text{B7f})$$

$$\tilde{C}_{1,n}(x) = 2C_F v(n) \mathcal{T}_1(x, y) \otimes \psi_n(y), \quad (\text{B7g})$$

$$\tilde{C}_{2,n}(x) = - \int_0^{\bar{x}} du \frac{\tilde{C}_{1,n}(u) - \tilde{C}_{1,n}(\bar{x})}{u - \bar{x}}. \quad (\text{B7h})$$

To derive the set of equations in (B7), we have used the relations between the amplitudes, which contain powers of L , and the various elements of the spectral density. These relations are given by

$$\text{Im} [T_0 \otimes (fL) \otimes \psi_n] = \ln \left(\frac{\bar{x}}{x} \right) C_{1,n}(f, x) + C_{2,n}(f, x), \quad (\text{B8})$$

$$\text{Im} [T_0 \otimes L^2 \otimes \psi_n] = \left[\ln^2 \left(\frac{\bar{x}}{x} \right) - \frac{\pi^2}{3} \right] \psi_n(x) + 2 \ln(x) C_{3,n}(x) - 2C_{4,n}(x), \quad (\text{B9})$$

where

$$C_{1,n}(f, x) = f(x, y) \otimes \psi_n(y),$$

$$C_{2,n}(f, x) = \int_0^{\bar{x}} du \frac{C_{1,n}(f, \bar{x}) - C_{1,n}(f, u)}{u - \bar{x}}.$$

-
- [1] B. Aubert *et al.* [BaBar Collaboration], Phys. Rev. D **80**, 052002 (2009).
 - [2] A. V. Efremov and A. V. Radyushkin, Theor. Math. Phys. **42**, 97 (1980).
 - [3] G. P. Lepage and S. J. Brodsky, Phys. Rev. D **22**, 2157 (1980).
 - [4] S. Uehara *et al.* [Belle Collaboration], Phys. Rev. D **86**, 092007 (2012).
 - [5] N. G. Stefanis, A. P. Bakulev, S. V. Mikhailov and A. V. Pimikov, Phys. Rev. D **87**, no. 9, 094025 (2013).
 - [6] A. E. Dorokhov, Phys. Part. Nucl. Lett. **7**, 229 (2010).
 - [7] A. V. Radyushkin, Phys. Rev. D **80**, 094009 (2009).
 - [8] M. V. Polyakov, JETP Lett. **90**, 228 (2009).
 - [9] H.-n. Li and S. Mishima, Phys. Rev. D **80**, 074024 (2009).
 - [10] S. V. Mikhailov and N. G. Stefanis, Nucl. Phys. B **821**, 291 (2009).
 - [11] A. P. Bakulev, S. V. Mikhailov, A. V. Pimikov and N. G. Stefanis, Phys. Rev. D **84**, 034014 (2011).
 - [12] A. P. Bakulev, S. V. Mikhailov, A. V. Pimikov and N. G. Stefanis, Phys. Rev. D **86**, 031501 (2012).
 - [13] S. J. Brodsky, F. G. Cao and G. F. de Teramond, Phys. Rev. D **84**, 033001 (2011).
 - [14] S. J. Brodsky, F. G. Cao and G. F. de Teramond, Phys. Rev. D **84**, 075012 (2011).
 - [15] K. Raya, L. Chang, A. Bashir, J. J. Cobos-Martinez, L. X. Gutiérrez-Guerrero, C. D. Roberts and P. C. Tandy, Phys. Rev. D **93**, no. 7, 074017 (2016).
 - [16] S. J. Brodsky and G. P. Lepage, Phys. Rev. D **24**, 1808 (1981).
 - [17] S. S. Agaev, V. M. Braun, N. Offen and F. A. Porkert, Phys. Rev. D **83**, 054020 (2011).
 - [18] S. S. Agaev, V. M. Braun, N. Offen and F. A. Porkert, Phys. Rev. D **86**, 077504 (2012).
 - [19] B. Wang, arXiv:1511.00373 [hep-ex].
 - [20] L. Chang, I. C. Cloet, J. J. Cobos-Martinez, C. D. Roberts, S. M. Schmidt and P. C. Tandy, Phys.

- Rev. Lett. **110**, no. 13, 132001 (2013).
- [21] N. G. Stefanis, Phys. Lett. B **738**, 483 (2014).
 - [22] N. G. Stefanis and A. V. Pimikov, Nucl. Phys. A **945**, 248 (2016).
 - [23] H. J. Behrend *et al.* [CELLO Collaboration], Z. Phys. C **49**, 401 (1991).
 - [24] J. Gronberg *et al.* [CLEO Collaboration], Phys. Rev. D **57**, 33 (1998).
 - [25] A. Denig [BESIII Collaboration], Nucl. Part. Phys. Proc. **260**, 79 (2015).
 - [26] P. Maris and P. C. Tandy, Phys. Rev. C **65**, 045211 (2002).
 - [27] P. Masjuan, Phys. Rev. D **86**, 094021 (2012).
 - [28] M. Hoferichter, B. Kubis, S. Leupold, F. Niecknig and S. P. Schneider, Eur. Phys. J. C **74**, 3180 (2014).
 - [29] A. P. Bakulev, S. V. Mikhailov and N. G. Stefanis, Phys. Lett. B **508**, 279 (2001); Erratum: [Phys. Lett. B **590**, 309 (2004)].
 - [30] B. Melić, D. Müller and K. Passek-Kumerički, Phys. Rev. D **68**, 014013 (2003).
 - [31] A. P. Bakulev, S. V. Mikhailov and N. G. Stefanis, Phys. Rev. D **67**, 074012 (2003).
 - [32] S. V. Mikhailov and A. V. Radyushkin, Nucl. Phys. B **273**, 297 (1986).
 - [33] K. A. Olive *et al.* (Particle Data Group), Chin. Phys. C **38**, 090001 (2014).
 - [34] A. Khodjamirian, Eur. Phys. J. C **6**, 477 (1999).
 - [35] S. V. Mikhailov and A. V. Radyushkin JETP Lett. **43**, 712 (1986).
 - [36] P. Gelhausen, A. Khodjamirian, A. A. Pivovarov and D. Rosenthal, Phys. Rev. D **88**, 014015 (2013); Erratum: [Phys. Rev. D **89**, 099901 (2014)]; Erratum: [Phys. Rev. D **91**, 099901 (2015)].
 - [37] S. V. Mikhailov and A. V. Radyushkin, Sov. J. Nucl. Phys. **49**, 494 (1989).
 - [38] A. P. Bakulev, S. V. Mikhailov and N. G. Stefanis, Annalen Phys. **13**, 629 (2004).
 - [39] H. M. Choi and C. R. Ji, Phys. Rev. D **91**, no. 1, 014018 (2015).
 - [40] V. M. Braun, S. Collins, M. Göckeler, P. Pérez-Rubio, A. Schäfer, R. W. Schiel and A. Sternbeck, Phys. Rev. D **92**, no. 1, 014504 (2015).
 - [41] V. M. Braun *et al.*, Phys. Rev. D **74**, 074501 (2006).
 - [42] R. Arthur, P. A. Boyle, D. Brömmel, M. A. Donnellan, J. M. Flynn, A. Jüttner, T. D. Rae and C. T. C. Sachrajda, Phys. Rev. D **83**, 074505 (2011).
 - [43] N. G. Stefanis, Nucl. Phys. Proc. Suppl. **181-182**, 199 (2008).
 - [44] A. P. Bakulev, S. V. Mikhailov, A. V. Pimikov and N. G. Stefanis, Nucl. Phys. Proc. Suppl. **219-220**, 133 (2011).
 - [45] N. G. Stefanis, S. V. Mikhailov and A. V. Pimikov, Few Body Syst. **56**, no. 6-9, 295 (2015).
 - [46] Y. N. Klopot, A. G. Oganesian and O. V. Teryaev, Phys. Lett. B **695**, 130 (2011).
 - [47] Y. N. Klopot, A. G. Oganesian and O. V. Teryaev, Phys. Rev. D **84**, 051901 (2011).
 - [48] Y. Klopot, A. Oganesian and O. Teryaev, Phys. Rev. D **87**, no. 3, 036013 (2013); Erratum: [Phys. Rev. D **88**, no. 5, 059902 (2013)].
 - [49] A. G. Oganesian, A. V. Pimikov, N. G. Stefanis and O. V. Teryaev, Phys. Rev. D **93**, no. 5, 054040 (2016).
 - [50] F. M. Dittes and A. V. Radyushkin, Phys. Lett. B **134**, 359 (1984).
 - [51] S. V. Mikhailov and A. V. Radyushkin, Nucl. Phys. B **254**, 89 (1985).
 - [52] A. V. Belitsky, A. Freund and D. Müller, Phys. Lett. B **493**, 341 (2000).